Electronic Supplementary Material (ESI) for Journal of Materials Chemistry C.

Supplementary Information

Balanced strain-dependent carrier dynamics in flexible organic-inorganic hybrid perovskites

Cheng Wang,[a] Lin Ma,*[a] Deqiang Guo,[a] Xin Zhao,[a] Zilin Zhou,[a] Dabin Lin,[a] Fangteng Zhang,[a] Weiren Zhao,[a] Jiahua Zhang[b] and Zhaogang Nie*[a]

[a]School of Physics and Optoelectronic Engineering, Guangdong University of Technology, Guangzhou, China

[b]State Key Laboratory of Luminescence and Applications, CIOMP, Chinese Academy of Sciences, Changchun, China

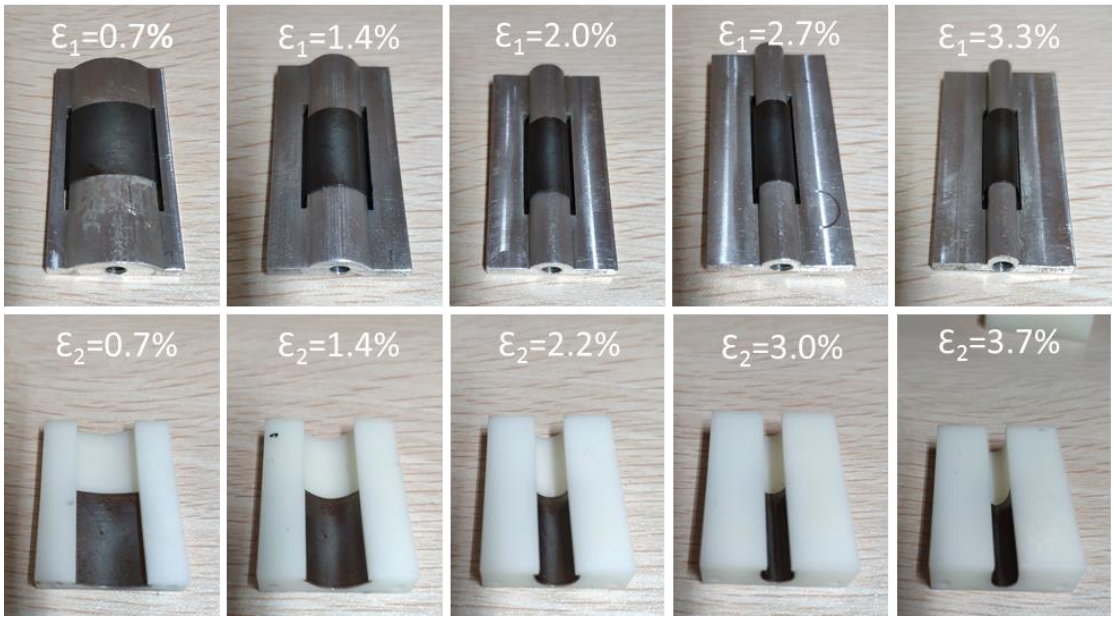

Fig. S1 Images of convex and concave bending molds (with perovskite film attached).

Table S1. The tensile (ε_1) or compressive (ε_2) strains applied and corresponding bending radius.

Convex bending	Bending radius *r* (mm)	12.75	6.50	4.42	3.38	2.75
	Tensile train ε_1 (%)	0.7	1.4	2.0	2.7	3.3
Concave bending	Bending radius *r* (mm)	12.25	6.00	3.92	2.88	2.25
	Compressive strain ε_2 (%)	0.7	1.4	2.2	3.0	3.7

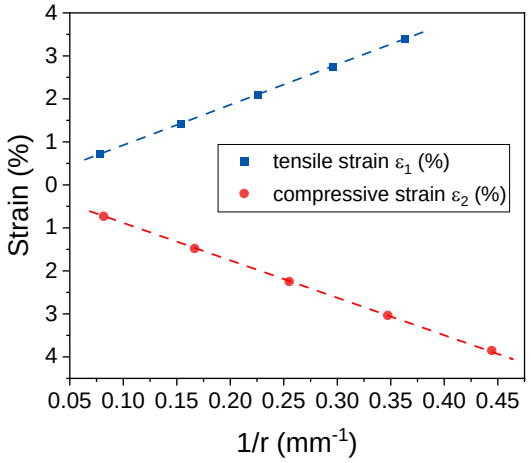

Figure S2. The relation between applied strain versus the reciprocal bending radius shown in table S1 (the dash lines are for eye guidance).

Table S2. Fitting parameters of time-resolve PL kinetics of $MAPbI_3$ film under different strain.

Strain	**τ_1 (ns)**	**A_1**	**τ_2 (ns)**	**A_2**	**τ_3 (ns)**	**A_3**	**$\tau_{average}$ (ns)**
ε_1=0%	1.71±0.01	0.80	13.7±0.2	0.17	199±3	0.03	9.32
ε_1=0.7%	1.64±0.01	0.79	13.2±0.2	0.18	177±3	0.03	9.10
ε_1=1.4%	1.78±0.01	0.74	15.6±0.2	0.21	195±2	0.05	13.54
ε_1=2.0%	1.92±0.02	0.74	16.8±0.2	0.22	172±3	0.04	12.59
ε_1=2.7%	2.12±0.02	0.71	17.2±0.2	0.24	180±2	0.05	14.84
ε_1=3.3%	2.47±0.02	0.62	20.9±0.2	0.30	164±2	0.07	19.83

ε_2=0.7%	1.03±0.01	0.80	11.7±0.4	0.14	141±2	0.07	12.14
ε_2=1.4%	1.20±0.02	0.81	11.3±0.4	0.14	141±3	0.06	10.67
ε_2=2.2%	1.14±0.01	0.84	10.5±0.3	0.13	140±4	0.04	7.27
ε_2=3.0%	1.13±0.01	0.84	10.1±0.3	0.13	145±4	0.03	6.85
ε_2=3.7%	1.24±0.01	0.84	10.3±0.3	0.14	137±6	0.02	5.63

The time-resolved PL kinetics were fitted using three-exponential decay equation (S1):

$$I(t) = B + A_1 \times e^{\frac{-t}{\tau_1}} + A_2 \times e^{\frac{-t}{\tau_2}} + A_3 \times e^{\frac{-t}{\tau_3}} \quad \text{(S1)}$$

where A_1, A_2, A_3 are the amplitudes of each decay component, and τ_1, τ_2, τ_3 are the decay time of each decay component. B is the background constant. The average lifetime $\tau_{average}$ is determined by the following equation:

$$\tau_{average} = \frac{A_1\tau_1 + A_2\tau_2 + A_3\tau_3}{A_1 + A_2 + A_3} \quad \text{(S2)}$$

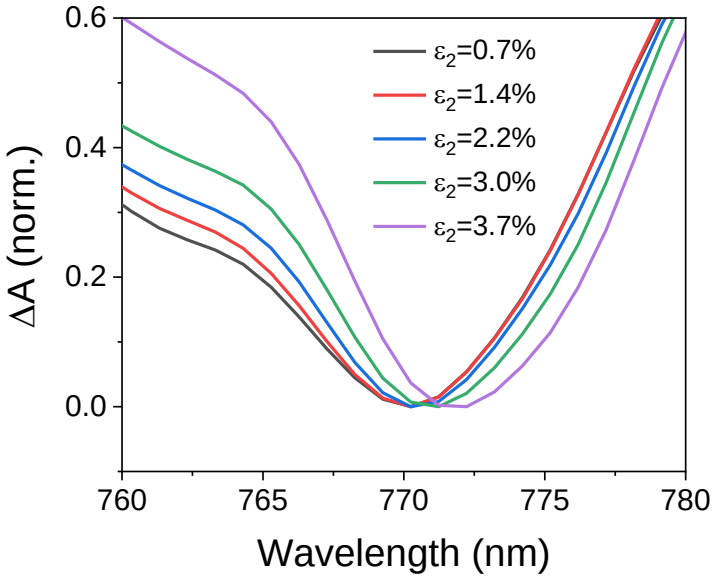

Fig. S3 Partial enlargement of transient absorption spectra of $MAPbI_3$ film at 9 ps after excitation (λ_{pump}=650 nm) under different compressive strains via concave bending.

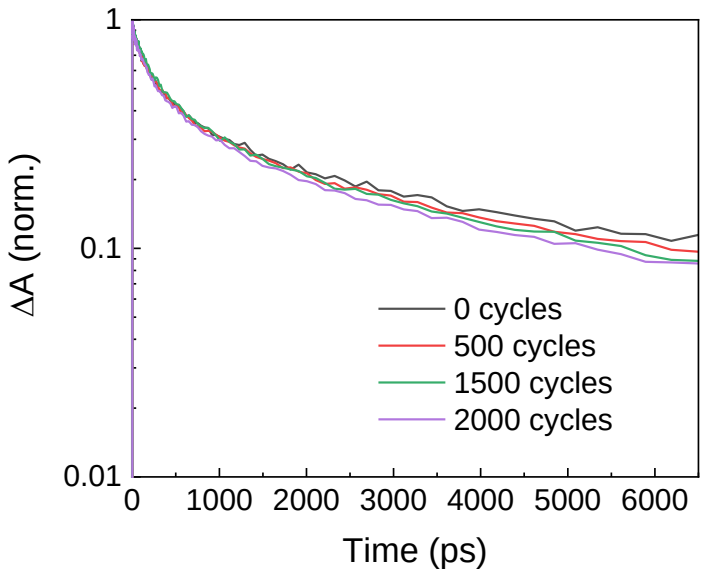

Fig. S4 Carrier dynamics in a flexible $MAPbI_3$ film versus bending cycles under convex bending radius of 1.1 mm.

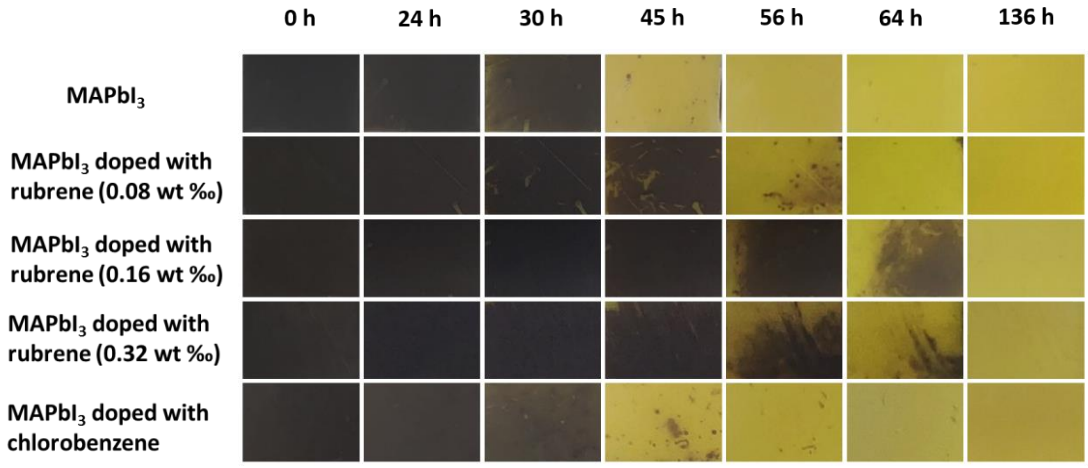

Fig. S5 Stabilities of $MAPbI_3$ film doped with rubrene at various concentrations.

The stabilities of rubrene doped $MAPbI_3$ films with various doping concentrations are shown in Figure S5. To investigate the influence of chlorobenzene solvent, the stability of $MAPbI_3$ film with adding chlorobenzene into the precursor solution was also recorded which shows no noticeable impact on the perovskite film stability.

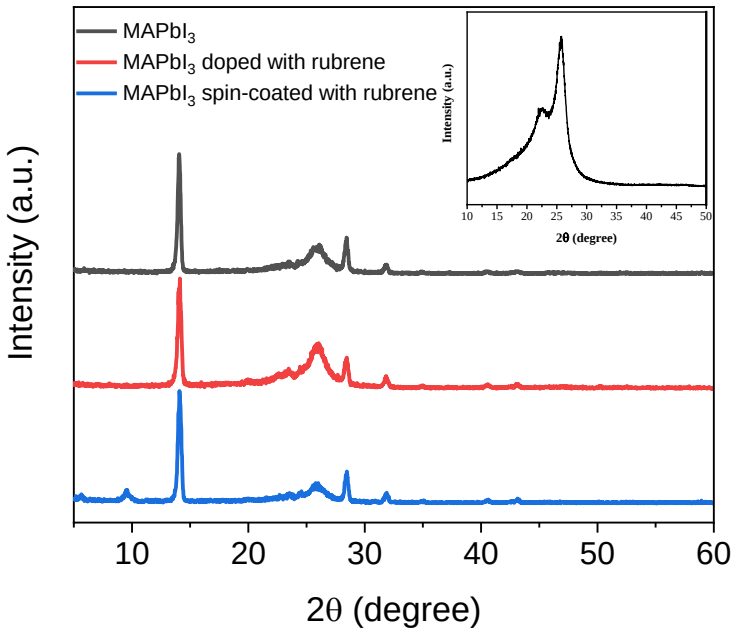

Fig. S6 GIXRD diffraction patterns of pristine $MAPbI_3$, $MAPbI_3$ doped with rubrene, and $MAPbI_3$ spin-coated with rubrene on PET films. The inset shows the GIXRD diffraction pattern of PET substrate.

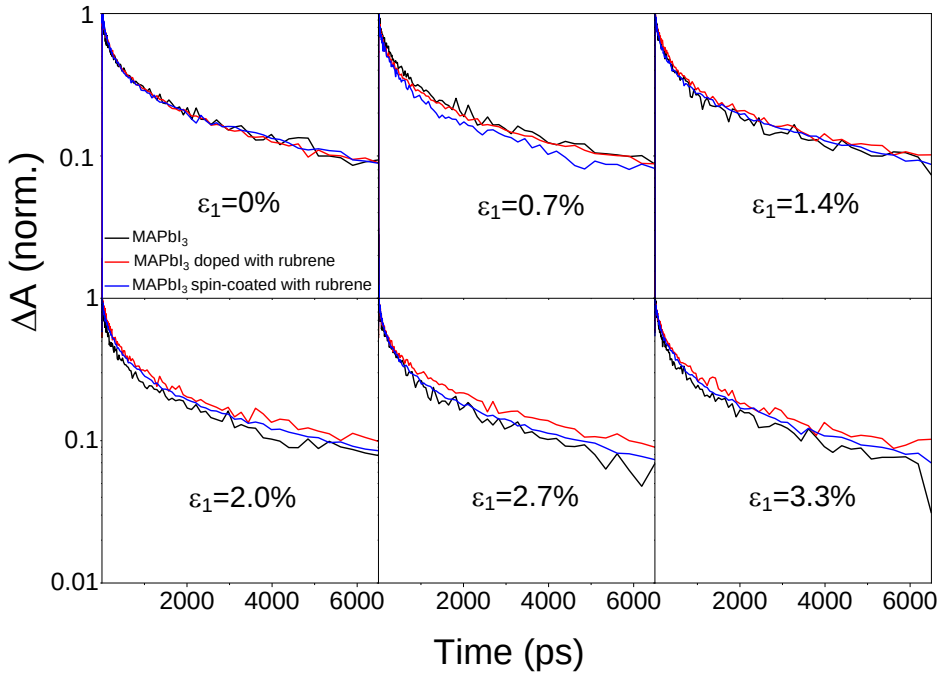

Fig. S7 TA kinetics at 760 nm of pristine $MAPbI_3$ (black), $MAPbI_3$ doped with rubrene (red), and $MAPbI_3$ spin-coated with rubrene (blue) films under various tensile strains.